Electronic Supplementary Material (ESI) for ChemComm.

Electronic Supplementary Information for

Carbon nanotube-encapsulated cobalt for oxygen reduction: Integration of space confinement and N-doping

Qichen Wang, Ke Ye, Liang Xu, Wei Hu, Yongpeng Lei, Yi Zhang, Yin Chen, Kechao Zhou, Jun Jiang, Jean M. Basset, Dingsheng Wang and Yadong Li*

Experimental Section

Synthesis of Co@NCNTs samples: Graphitic carbon nitride (g-C_3N_4) was prepared by treating melamine at 550 °C in air for 4 h. The Co@NCNTs samples were prepared by one-step solid-state reaction. Typically, Typically, $Co(NO_3)_2 \cdot 6H_2O$ (0.01g), g-C_3N_4 (0.5g) and glucose (0.1g) were firstly mixed, obtaining the homogeneous yellow powder.. Then homogeneous yellow powder was transferred into the center of tube furnace, followed by carbonation at 700~900 ^oC for 1 h. Finally, the as-prepared black powder was then washed with 0.5 M H_2SO_4 for 8 h to remove the unstable Co species, followed by drying at 80 °C overnight. The Co@NCNTs was collected for further test or characterization.

Characterization: The crystal phases were identified by X-ray diffraction (XRD, Bruker AXS D8 ADVANCE) with Cu Kα (λ =1.5406 Å) radiation at a scanning rate of 2θ= 0.02° per step. X-ray photoelectron spectra (XPS) were recorded on a Thermo Scientific ESCALAB 250 Xi machine with an Al Kα source. The morphology and structure of the samples were characterized by high-resolution transmission electronmicroscope HRTEM, (JEM-2100) operated at 200 kV and scanning electron microscope (SEM, Quanta 450 ESEM, FEI) operated at 10 kV. Raman measurements were performed on Bruker RAM II with a laser wavelength of 532 nm. The specific surface area and the pore size distribution of the samples were estimated from nitrogen adsorption isotherm (ASAP 2020 at 77 K, USA) by means of the Brunauer-Emmett-Teller (BET) equation and the Barrett-Joyner-Halenda (BJH) model, respectively. The X-ray absorption find structure spectra (Co K-edge) were collected at BL1W1B station in Beijing Synchrotron Radiation Facility (BSRF, the storage rings were operated at 2.5 GeV with a maximum current of 250 mA). The data were collected at room temperature in transmission mode using N_2-filled ionization chamber (Si (111) monochromator for Co K-edge).

Electrochemical measurements: The electrochemical measurements were performed in a three-electrode cell using a rotating disk electrode with a CHI 660e workstation

(CHI 660e, Chenhua, China) at 25 °C, which Pt wire and a SCE electrode (saturated KCl-filled) as a counter electrode and the reference electrode, respectively. All of the potentials in this work were calibrated to the reversible hydrogen electrode (RHE) according to Nernst equation. In brief, The catalyst ink was prepared by dispersing 5mg of catalyst in 1 ml of water-isopropanol solution(V:V = 3:1) containing 40 μL Nafion solution, sonicating for at least 60 min. Then 5 μL catalyst ink was pipetted onto the glassy carbon electrode. Before testing, N_2/O_2 were bubbled into KOH solution at least 30 min to ensure N_2/O_2 saturation. The cyclic voltammograms (CVs) were measured in N_2/O_2-saturated KOH solution. RDE tests were measured in O_2-saturated 0.1 M KOH with a scan rate of 50 mV s^{-1}. And linear sweep voltammetry curves (LSVs) data were collected with a rotating speed range from 400 to 2500 rpm on RDE with a scan rate of 5 mV s^{-1}.

In order to estimate the four-electron selectivity of catalysts, the electron transfer number was calculated based on Koutecky-Levich (K-L) equation.

$$\frac{1}{j}=\frac{1}{j_L}+\frac{1}{j_k}=\frac{1}{B\omega^{1/2}}+\frac{1}{j_k} \qquad B=0.2nFC_0(D_0)^{2/3}v^{-1/6} \qquad j_k=nFkC_0$$

Here, j, j_k and j_L represent the measured current density, the kinetic- and diffusion-limiting current densities, respectively; ω is the disc rotation angular velocity of the disk, n represents calculated number of transferred electron in ORR; F is the Faraday constant (F =96485 C mol^{-1}); C_0 is the bulk concentration for O_2 (1.2×10^{-6} mol cm^{-3}) dissolved in 0.1 M KOH solution; D_0 is the diffusivity of O_2 (1.9×10^{-5} cm^2 s^{-1}); v is the kinematic viscosity of electrolyte, and k is the electron-transferred rate constant.

For methanol crossover tests, the chronoamperometric response at 0.8 V is recorded by RDE tests with a rotation rate of 1600 rpm and followed by the introduction of 0.5 M methanol into the electrolyte. Stability test was performed at 0.8 V in RDE measurement for 100,000s.

The CV curves were recorded in O_2-satuated 0.1 M KOH at scan rates of 5, 10, 15, 20, 25, and 30 mV s^{-1}, separately. The capacitive current measured at 1.05 V (vs. RHE) was plotted as a function of the different scan rate.

The electrocatalytic OER activity was performed in 1 M KOH solution. The

catalyst ink was dropped into the GC electrodes (8.0 mm inner diameter). LSVs for the OER are obtained in 1 M KOH solution at a scan rate of 2 mV s^{-1}. The low scan rate is mainly in order to reduce the capacitive current.

Zn-air batteries measurements:

The Co@NCNTs based-air electrodes used for Zn-air batteries were composed of a stainless steel mesh (SSM) and a gas diffusion layer (GDL) on the air-facing side as well as a catalyst ink layer (CIL) on the water-facing side. Firstly, the GDL was constructed by carbon black dispersed in ethanol, and followed by dropping PTFE emulsion with a mass ratio of PTFE emulsion to carbon black of 7:3. After stirring for 1 h and drying at 80 °C overnight to remove excess ethanol, the obtained dough-like paste was rolled to form a film of 0.25 mm thickness. Next, the film was rolled onto SSM (mesh 40 × 40, type 304), and then sintered at 360 °C for 1h. The CIL was prepared by loading catalyst ink onto the other side of the SSM by drop-casting method. The catalyst loading is 1.0 mg cm^{-2}. Electrochemical reactors with total volume of 28 mL were constructed to test the primary Zn-air batteries. A polished zinc plate of 0.3 mm thickness and 6 M KOH were used as anode electrolyte for Zn-air batteries. The specific capacity and gravimetric energy density were achieved when normalized to the mass of consumed Zn during test.[1]

For the rechargeable Zn-air batteries, the electrolyte used is 6 M KOH with 0.2 M Zn acetate to ensure reversible Zn electrochemical reactions at the anode. The galvanostatic discharge (ORR) and discharge-charge (ORR-OER) cycling stability were carried out by LAND testing system. Both the discharge or charge current and corresponding power densities were normalized to the effective surface area of air-cathode electrode. The specific capacity was calculated according to the equation:

$$\frac{\text{current} \times \text{service hours}}{\text{weight of consumed zinc}}$$

The energy density was calculated according to the equation:

$$\frac{\text{current} \times \text{service hours} \times \text{average discharge voltage}}{\text{weight of consumed zinc}}$$

Computational details and methods

All electronic structures calculations were performed using PBE functional [2] and the plan-wave projector augmented wave (PAW) [3] method with an energy cut-off of 450 eV, as implemented Vienna ab initio Simulation Package (VASP).[4, 5] The GGA+U method was applied to describe partially filled d-orbitals by considering coulomb and exchange corrections.[6] Van der Waals (vdW) correction is applied in all calculations.[7] All geometric structures were fully relaxed until energy and forces were converged to 10^{-4} eV and 0.01 eV $Å^{-1}$, respectively. The lattice constants of these models are 12.5Å×12.7Å×17.9Å. The Brillouin zone was sampled with 3×3×1 Monkhorst-Pack k-meshes for the geometry optimization.

Reaction mechanism

The overall O_2 reduction reaction (ORR) to OH^- in alkaline environment is:

$$O_2 + 2H_2O + 4e^- \longrightarrow 4OH^-$$

The proposed mechanism of ORR in alkaline solution consist of three (one dissociative and two associative) possible reaction pathways (Scheme 1)[8]

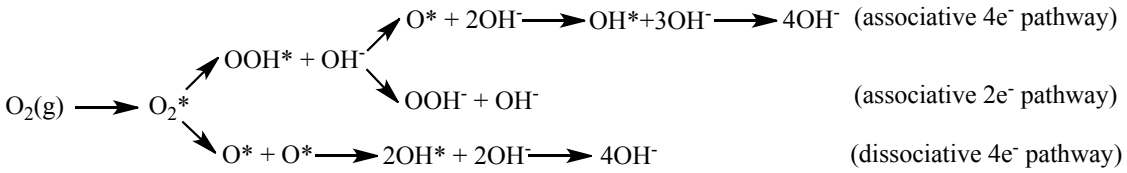

Scheme 1: Possible reaction pathways of ORR in alkaline solution.

Specifically, previous first principle study showed that dissociation pathway does not exist on graphitic nitrogen-doped graphene surface, since the surface of a doped graphene features the relatively high energy barrier (>1.2 eV) in the dissociative pathway.[8, 9, 10]

The following associative mechanism is dominant and considered in our calculation:

(1a) $O_2(g) + H_2O(l) + e^- + * \longrightarrow OOH^* + OH^-$

(1b) $OOH^* + e^- \longrightarrow O^* + OH^-$

(1c) $O^* + H_2O(l) + e^- \longrightarrow OH^* + OH^-$

(1d) $OH^* + e^- \longrightarrow OH^- + *$

where * stands for an active site on the catalytic surface, (l) and (g) refer to liquid and gas phases, respectively.

Free Energy Change

The chemical potential of each adsorbate is defined as:

$$\mu = E + E_{ZPE} - T \times S$$

It is difficult to obtain the exact free energy of OOH, O, and OH radicals in the electrolyte solution, the adsorption free energy ΔG_{O^*}, ΔG_{OH^*} and ΔG_{OOH^*}, are relative to the free energy of stoichiometrically appropriate amounts of $H_2O(g)$ and $H_2(g)$, defined as follows:

$$\Delta G_{OH^*} = \Delta G\left(H_2O(g) + * \rightarrow OH^* + 1/2H_2(g)\right)$$

$$= \mu_{OH^*} + 0.5 \times \mu_{H_2} - \mu_{H_2O} - \mu_*$$

$$= \left(E_{OH^*} + 0.5 \times E_{H_2} - E_{H_2O} - E_*\right) + \left(E_{ZPE(OH^*)} + 0.5 \times E_{ZPE}\right.$$

$$- T \times (S_{OH^*} + 0.5 \times S_{H_2} - S_{H_2O} - S_*)$$

$$\Delta G_{OOH^*} = \Delta G\left(2H_2O(g) + * \rightarrow OOH^* + 3/2H_2(g\right.$$

$$= \mu_{OOH^*} + 1.5 \times \mu_{H_2} - 2 \times \mu_{H_2O} - \mu_{}$$

$$= \left(E_{OOH^*} + 1.5 \times E_{H_2} - 2 \times E_{H_2O} - E_*\right) + \left(E_{ZPE(OOH^*)} + 1.5\right.$$

$$- T \times (S_{OOH^*} + 1.5 \times S_{H_2} - 2 \times S_{H_2O} - S_*)$$

$$\Delta G_{O^*} = \Delta G\left(H_2O(g) + * \rightarrow O^* + H_2(g)\right)$$

$$= \mu_{O^*} + \mu_{H_2} - \mu_{H_2O} - \mu_*$$

$$= \left(E_{O^*} + E_{H_2} - E_{H_2O} - E_*\right)$$

$$+ \left(E_{ZPE(O^*)} + E_{ZPE(H_2)} - E_{ZPE(H_2O)} - E_{ZPE(*)}\right)$$

$$- T \times (S_{O^*} + S_{H_2} - S_{H_2O} - S_*)$$

The change of free energy (ΔG) for all reaction is defined by following equation: $\Delta G=\Delta E + \Delta ZPE - T\Delta S + \Delta G_U + \Delta G_{pH}$. The ΔE, ΔZPE and ΔS are the different energy, zero-point energy, and entropy of the reaction, respectively. The ΔE is obtained from analyzing the DFT total energies. The ΔS is the entropy difference between the adsorbed state ant the gas phase. The T is of room temperature 298.15K. The ΔZPE of adsorbed species were obtained from harmonic vibrational frequency calculations. Only adsorbed species vibrational modes were calculated explicitly, while the functionalized N-doped graphene sheets were fixed (assuming vibrations of the embedded N-doped graphene sheets are negligible), as done in previous theoretical studies.[11-15] The entropies of adsorbed species were neglected. The entropies and vibrational frequencies of molecules in the gas phase were taken from the NIST database.[16] Given that the high-spin ground state of the oxygen molecule is poorly described in DFT calculations. The free energy of O_2 was derived as $G(O_2) = 2G(H_2O) – 2G(H_2)$ - 4.92 eV from the free energy change of the reaction $O_2 + 2H_2 \rightarrow 2H_2O$ which is 4.92 eV under the standard condition. To calculate the free energy of OH^- , we assume that $H_2O(l) \rightarrow H^+ + OH^-$, $\Delta G = 0$ (U=0, pH=0, p=1bar, T=298K). Then, $G(OH^-) = G(H_2O) – 1/2G(H_2)$. The $G(H^+)$ is defined as $1/2G(H_2)$.[17] Therefore, $G(OH^-) = G(H_2O) - 1/2\ G(H_2)$. $\Delta G_U = -eU$, in which U is the potential related to the RHE. $\Delta G_{pH} = -kTln10*pH$, which is the correction free energy of OH^- ions depended by the concentration. The value of ΔG_{1a}, ΔG_{1b}, ΔG_{1c}, and ΔG_{1d} is obtained at U= 0 V, pH =13 (the experimental environment for ORR) for above equations. The equilibrium potential (U^{equil}) for ORR is obtained by $U^{equli} = 1.23-kTln10*pH = 0.462$. The barrier for ORR ($E_{barrier}$) at equilibrium potential is then obtained by $E_{barrier} = \max\{\Delta G_{1a}, \Delta G_{1b}, \Delta G_{1c}, \Delta G_{1d}\} + U^{equil} *e = \max\{\Delta G_{1a}, \Delta G_{1b}, \Delta G_{1c}, \Delta G_{1d}\} + 0.462$.

The reaction free energy of equations (1a)–(1d) (ΔG_1, ΔG_2, ΔG_3, ΔG_4) for ORR can be calculated using the following equations:

$$\Delta G_1 = \mu_{OOH^*} + \mu_{OH^-} - \mu_{H_2O} - \mu_* - \mu_{O_2} - \mu_{e^-}$$

$$= \mu_{OOH^*} + \left(\mu_{H_2O} - \mu_{H^+}\right) - \mu_{H_2O} - \mu_* - \left(2\mu_{H_2O} - 2\mu_{H_2} + 4 \times 1.23\right) - \mu_{e^-}$$

$$= \mu_{OOH^*} + 1.5 \times \mu_{H_2} - 2 \times \mu_{H_2O} - \mu_* - 4.92$$

$$= \Delta G_{OOH^*} - 4.92$$

$$\Delta G_2 = \mu_{O^*} + \mu_{OH^-} - \mu_{OOH^*} - \mu_{e^-}$$

$$= \mu_{O^*} + \left(\mu_{H_2O} - \mu_{H^+}\right) - \mu_{OOH^*} - \mu_{e^-}$$

$$= \mu_{O^*} + \mu_{H_2O} - 0.5 \times \mu_{H_2} - \mu_{OOH^*}$$

$$= \left(\mu_{O^*} + \mu_{H_2} - \mu_{H_2O} - \mu_*\right) - \left(\mu_{OOH^*} + 1.5 \times \mu_{H_2} - 2 \times \mu_{H_2O} - \mu_*\right)$$

$$= \Delta G_{O^*} - \Delta G_{OOH^*}$$

OH(XXXXXXXXXXXXXXXXXXXXXXXXXXXXXXXXXXXXXXXXXXXXXXX
XXXXXXXXXXXXXXXXXXXXXXXXXXXXXXXXXXXXXXXXXXXX
XXXXXXXXXXXXXXXXXXXXXXXXXXXXXXXXXXXXXXXXXXXX
XXXXXXXXXXXXXXXXXXXXXXXXXXXXXXXXXXXXXXXXXXXX
XXXXXXXXXXXXXXXXXXXXXXXXXXXXXXXXXXXXXXXXXXXX
XXXXXXXXXXXXXXXXXXXXXXXXXXXXXXXXXXXXXXXXXXXX
XXXXXXXXXXXXXXXXXXXXXXXXXXXXXXXXXXXXXXXXXXXX
XXXXXXXXXXXXXXXXXXXXXXXXXXXXXXXXXXXXXXXXXXXX
XXXXXXXXXXXXXXXXXXXXXXXXXXXXXXXXXXXXXXXXXXXX
XXXXXX$\Delta G_3 = \mu_{OH^*} + \mu_{OH^-} — \mu_{O^*} - \mu_{H_2O} - \mu_{e^-}$

$$= \mu_{OH^*} + \left(\mu_{H_2O} - \mu_{H^+}\right) - \mu_{O^*} - \mu_{H_2O} - \mu_{e^-}$$

$$= \mu_{OH^*} - 0.5 \text{ x } \mu_{H_2} - \mu_{O^*}$$

$$= \left(\mu_{OH^*} + 0.5 \text{ x } \mu_{H_2} - \mu_{H_2O} - \mu_*\right) - \left(\mu_{O^*} + \mu_{H_2} - \mu_{H_2O} - \mu_*\right)$$

$$= \Delta G_{OH^*} - \Delta G_{O^*}$$

$$\Delta G_4 = \mu_{OH^-} + \mu_* - \mu_{OH^*} - \mu_{e^-}$$

$$= \left(\mu_{H_2O} - \mu_{H^+}\right) + \mu_* - \mu_{OH^*} - \mu_{e^-}$$

$$= \mu_{H_2O} - 0.5 \text{ x } \mu_{H_2} + \mu_* - \mu_{OH^*}$$

$$= -\left(\mu_{OH^*} + 0.5 \times \mu_{H_2} - \mu_{H_2O} - \mu_*\right)$$

$$= - \Delta G_{OH^*}$$

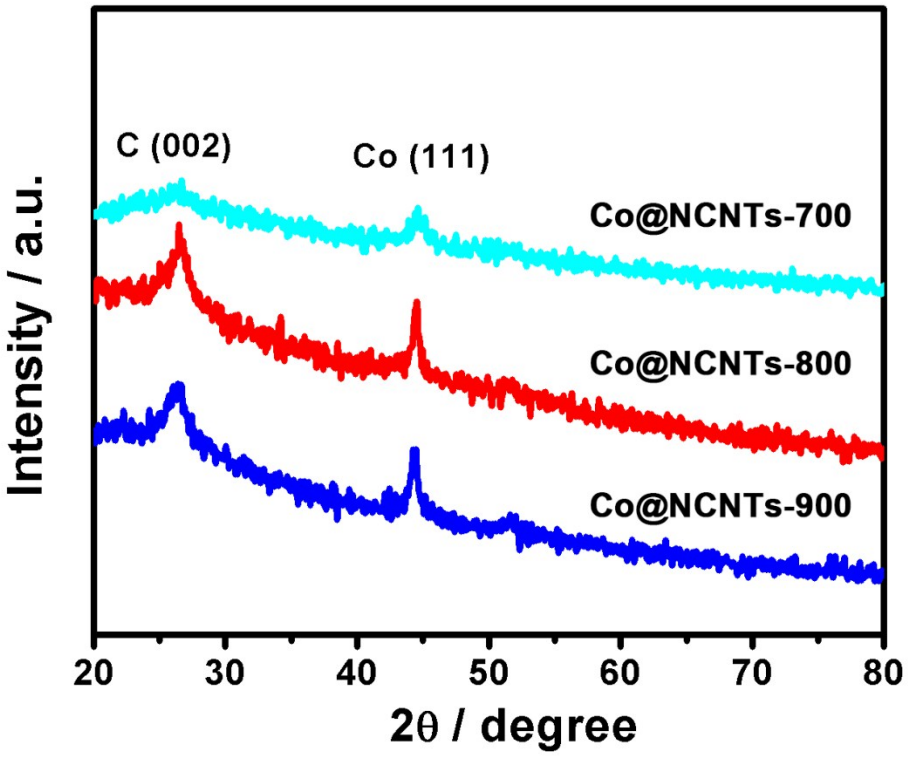

Fig. S1 XRD patterns of Co@NCNTs samples.

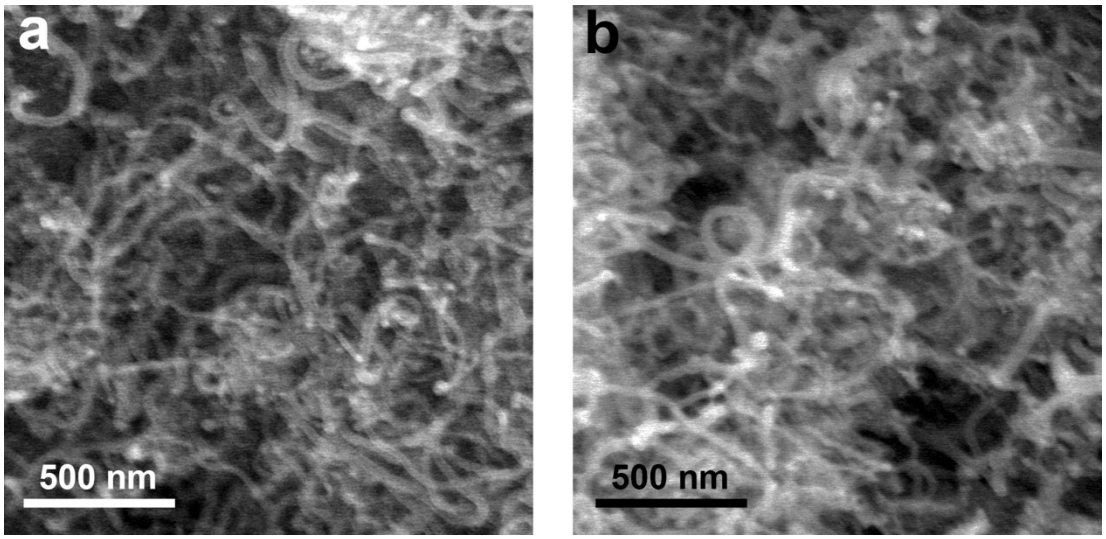

Fig. S2 SEM images of (a) Co@NCNTs-700 and (b) Co@NCNTs-900.

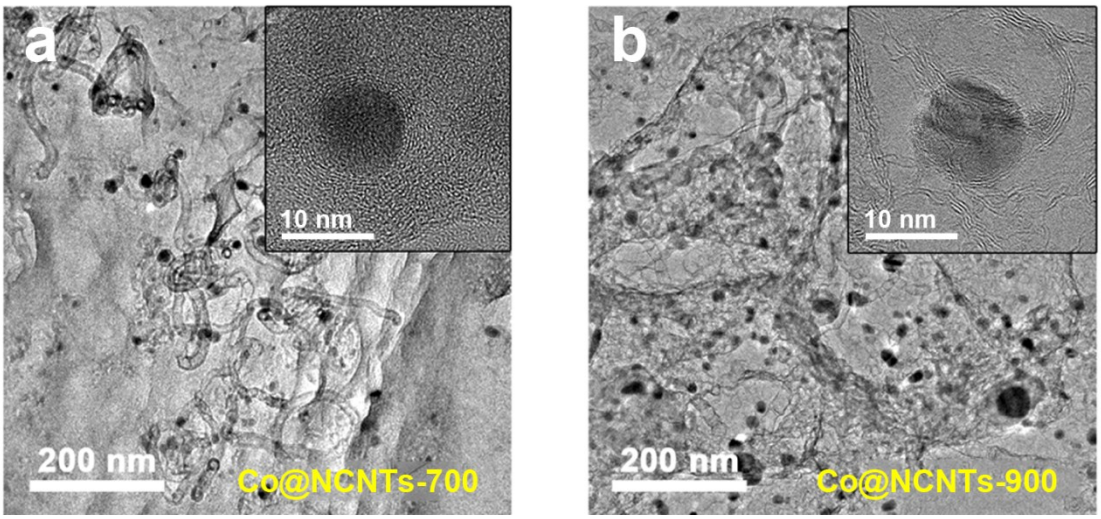

Fig. S3 TEM images of (a) Co@NCNTs-700 and (b) Co@NCNTs-900. Inset shows the corresponding HRTEM image.

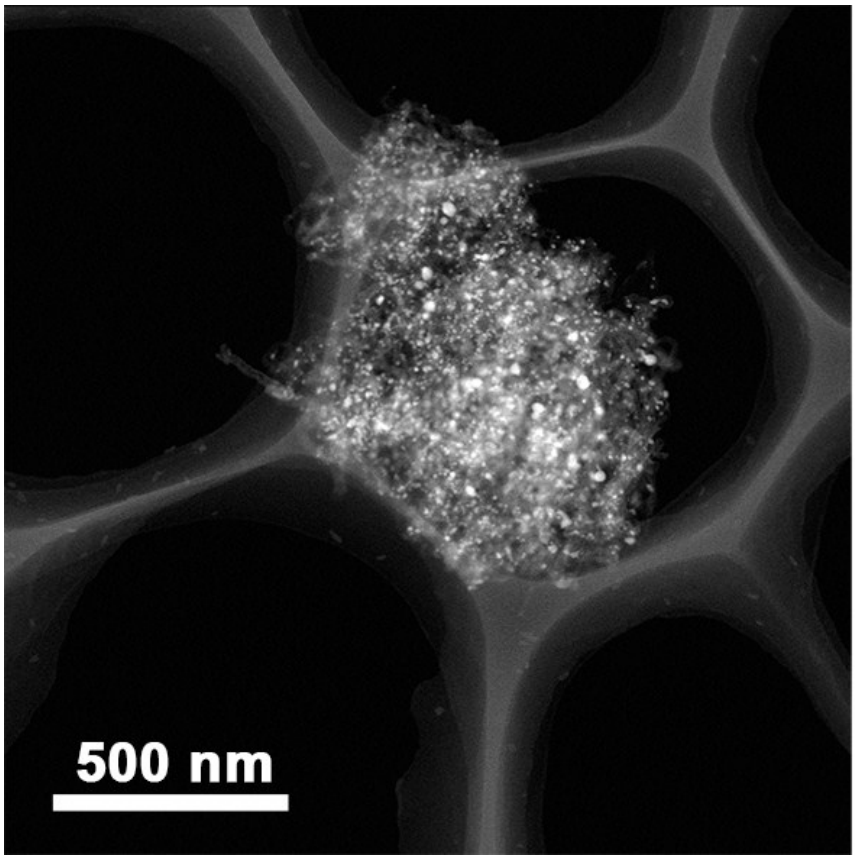

Fig. S4 STEM image for Co@NCNTs-800.

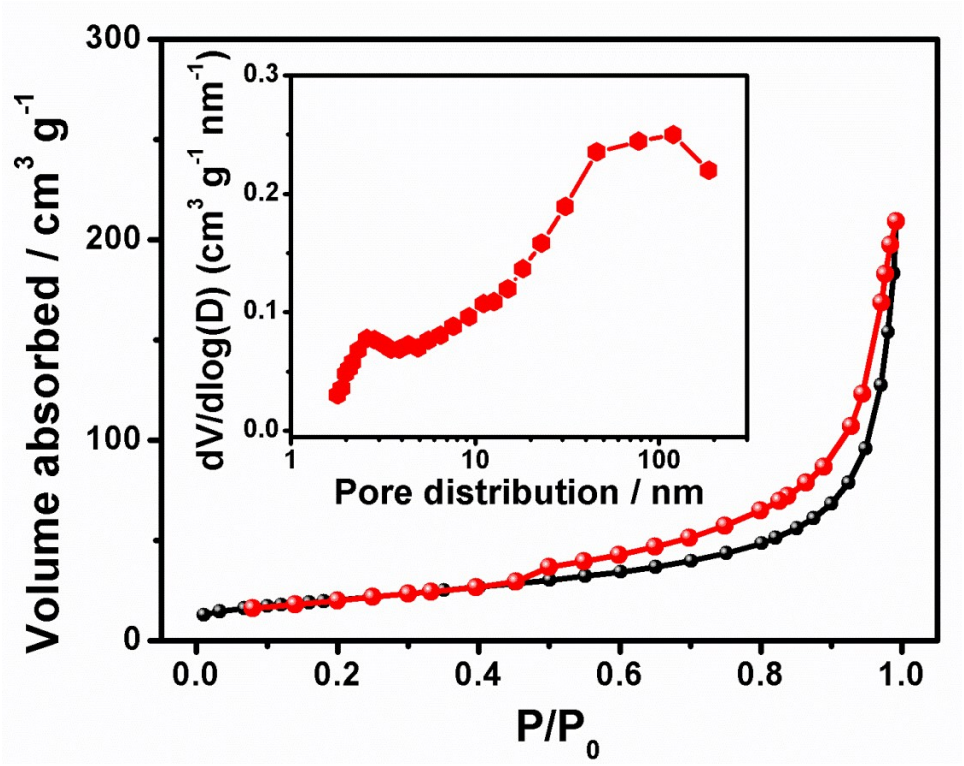

Fig. S5 N_2 adsorption/desorption isotherms of Co@NCNTs-800.

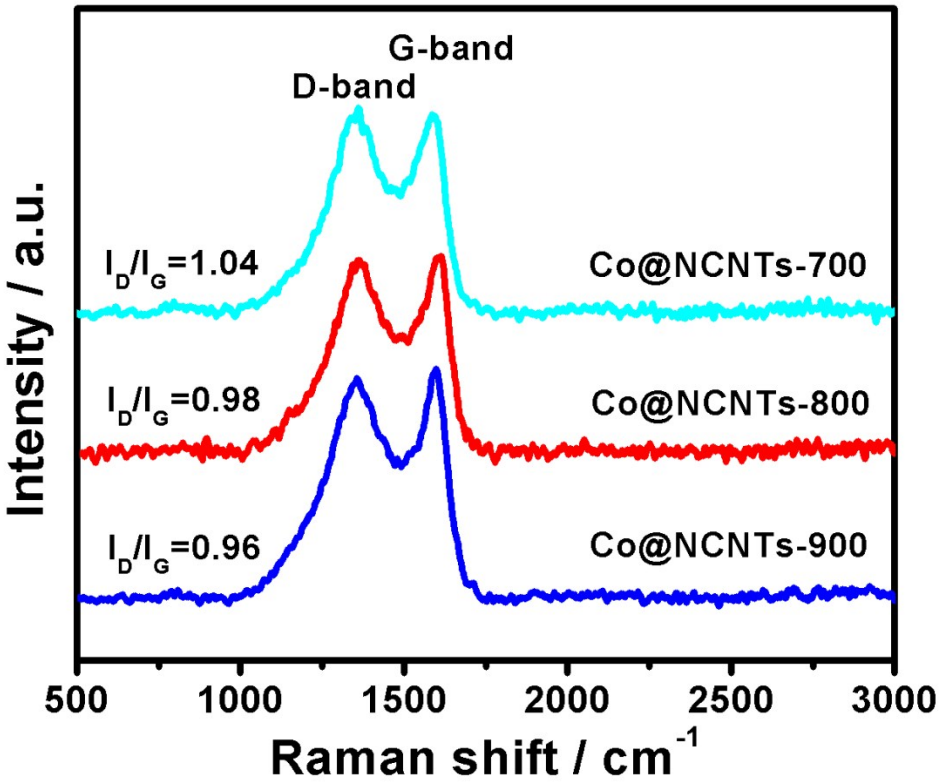

Fig. S6 Raman spectra of Co@NCNTs samples.

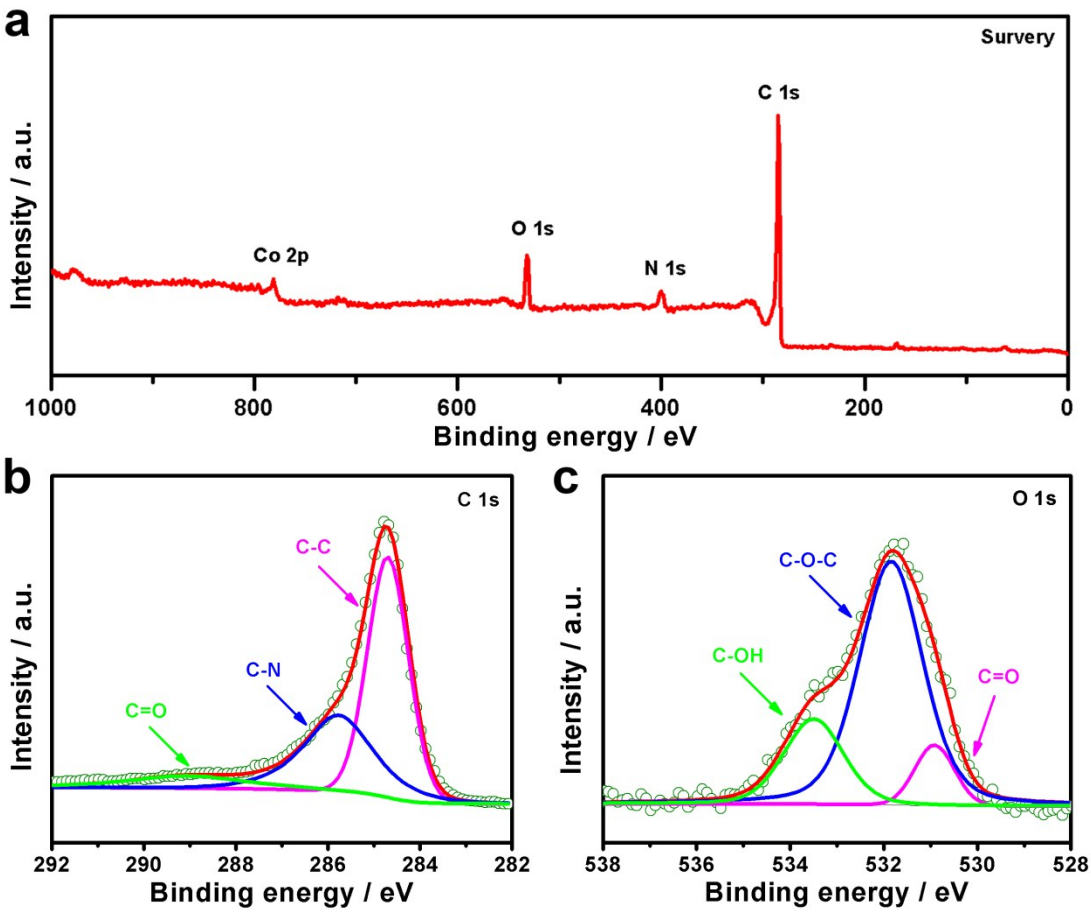

Fig. S7 (a) XPS survey spectrum. (b) High-resolution C 1s. (c) High-resolution O 1s XPS spectrum of Co@NCNTs-800.

The C 1s peak of Co@NCNTs-800 can be deconvoluted into by three peaks (Fig. S7b), which can be assigned to sp^2-hydridized C-C (284.7 eV), C-N (285.8 eV) and C=O (288.9 eV), respectively. The existence of C-N bond confirmed the N species have been doped in the carbon framework, optimizing the adsorption of the oxygenated species (*e.g.*, O_2 and OH^-). And some hydrophilic oxygen-containing-groups (e.g. C=O, C–O–C and C–OH) were found in Fig. S7c, which undoubtedly enhances the hydrophilicity ability towards catalysts-electrolyte interaction.

.

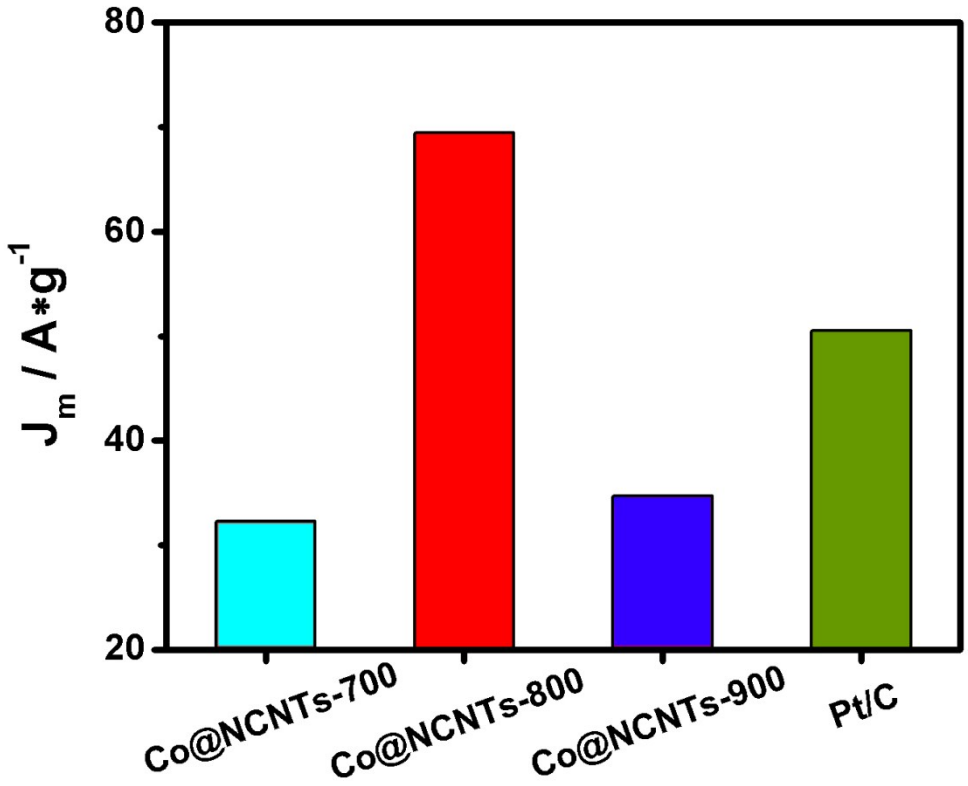

Fig. S8 The mass activities of the Co@NCNTs and Pt/C samples at 0.80 V.

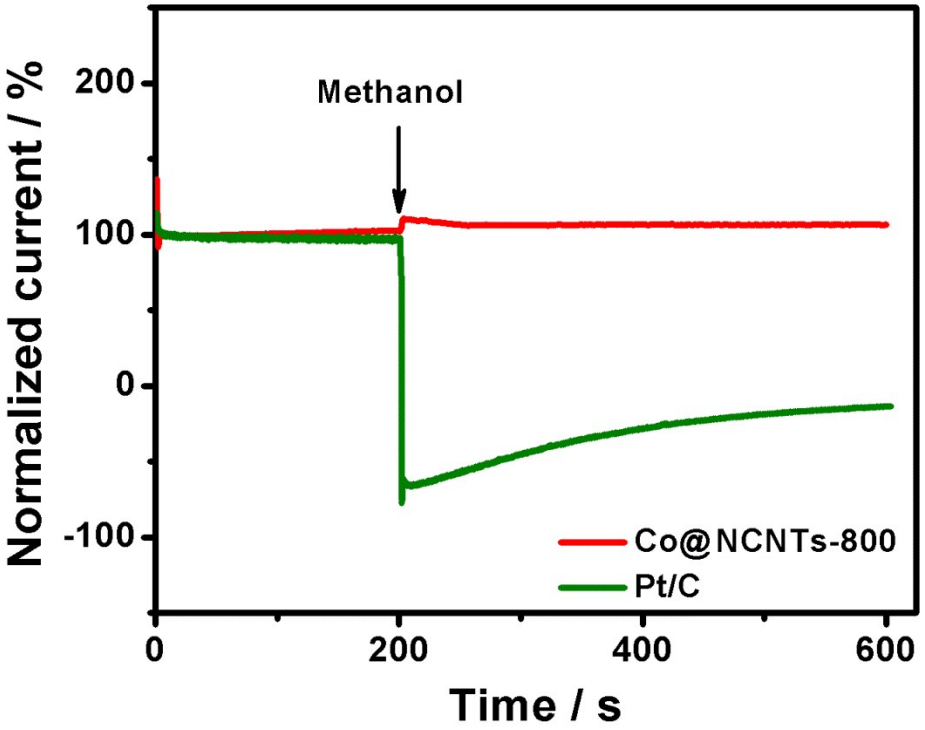

Fig. S9 Chronoamperometric response to test methanol crossover effect.

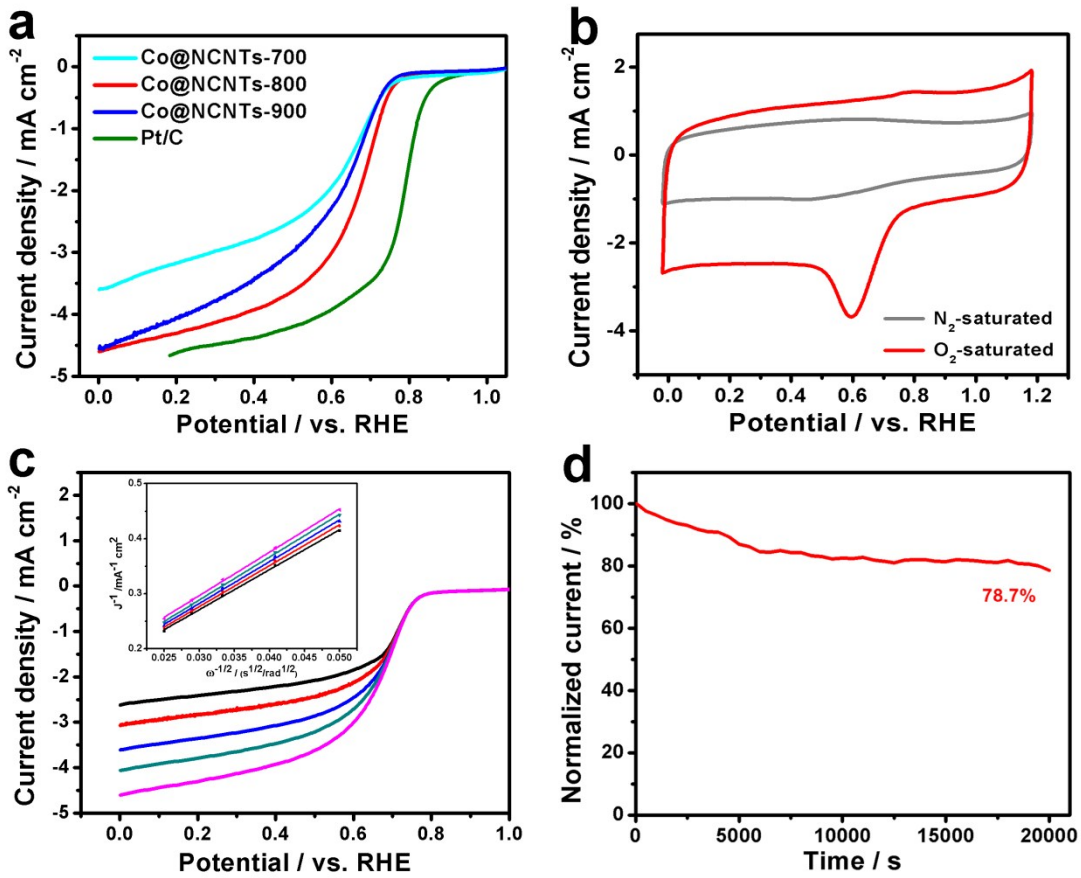

Fig. S10 (a) LSV curves for Co@NCNTs samples at 1600 rpm measured in 0.5 M H_2SO_4. Scan rate: 5 mV s^{-1}. (b) CVs curves of Co@NCNTs-800. (c) LSV curves of Co@NCNTs-800 at different rotation speed. Inset shows the fitted K-L plots. (d) Long-term stability. In 0.5 M H_2SO_4, Co@NCNTs-800 also exhibits reasonable ORR activity (E_{onset}: 0.79 V; $E_{1/2}$:0.63 V) in comparison to commercial Pt/C. And the electron transfer number (n) for Co@NCNTs-800 was typical $4e^-$ pathway. Moreover, the i-t curve shows only 21.3% current decrease of initial activity for the Co@NCNTs-800 catalyst after 20000 s.

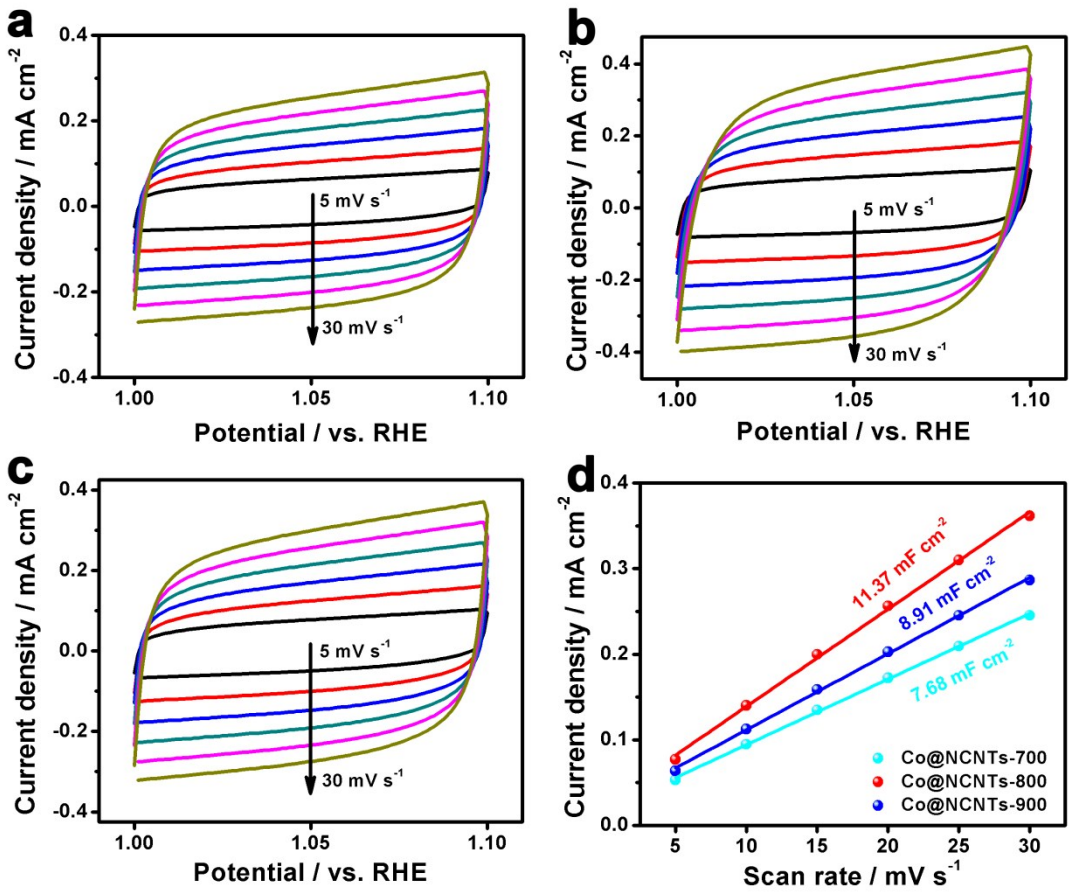

Fig. S11 (a) CVs curves for (a) Co@NCNTs-700, (b) Co@NCNTs-800, (c) Co@NCNTs-900 at scan rates of 5, 10, 15, 20, 25 and 30 mV s^{-1} measured in O_2-satuated 0.1 M KOH. (d) The capacitive current measured at 1.05 V vs RHE was plotted as a function of scan rate for Co@NCNTs samples.

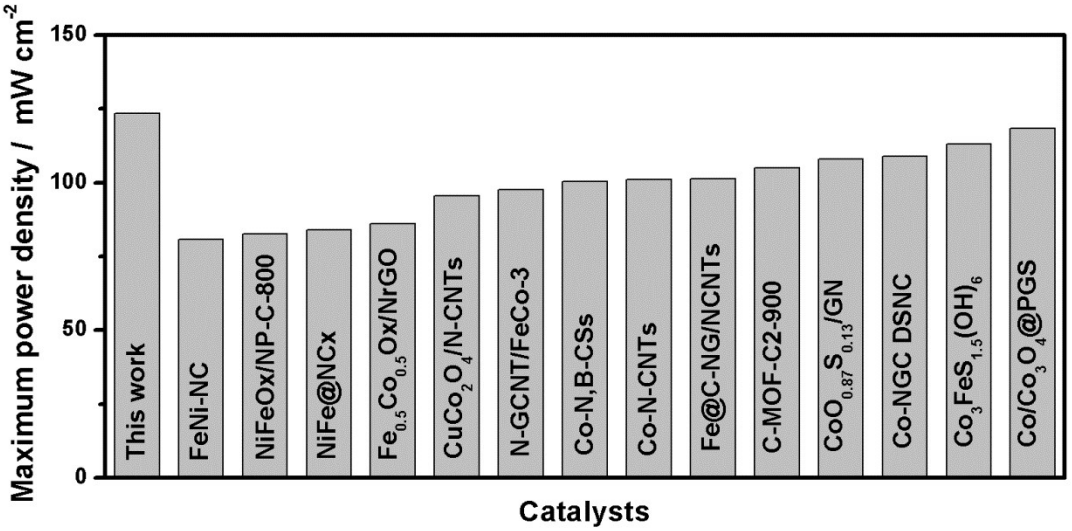

Fig. S12 Comparsion of maximum power density of Co@NCNTs-800 and other advanced catalysts reported.[18-31]

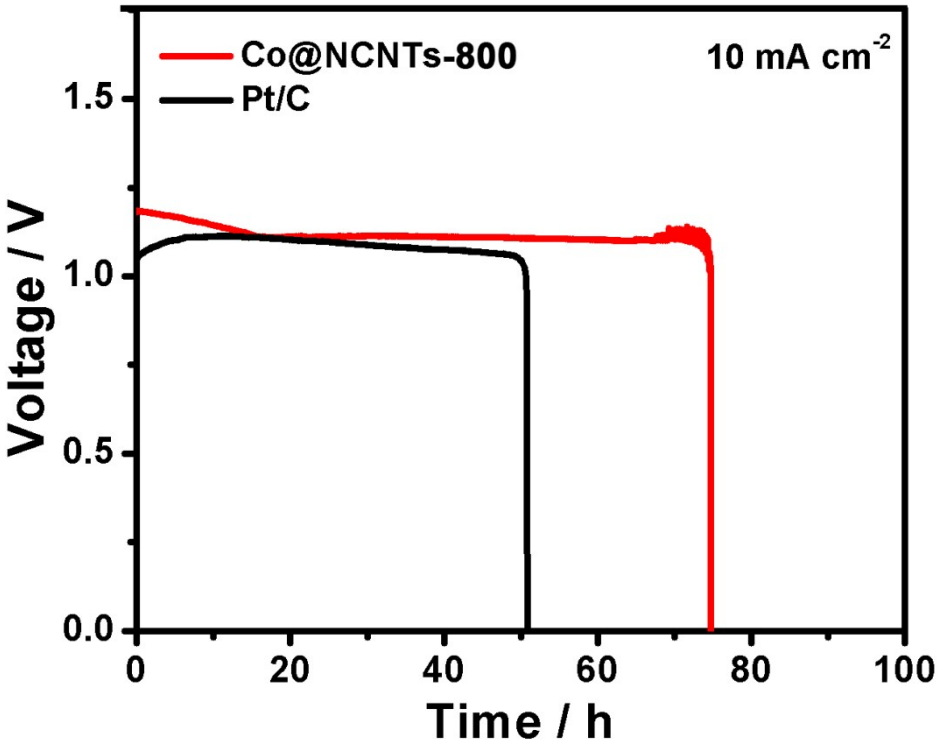

Fig. S13 Long-time discharge curve of a primary Zn-air batteries was assembled using Co@NCNTs-800 and Pt/C cathode at current densities of 10 mA cm^{-2}.

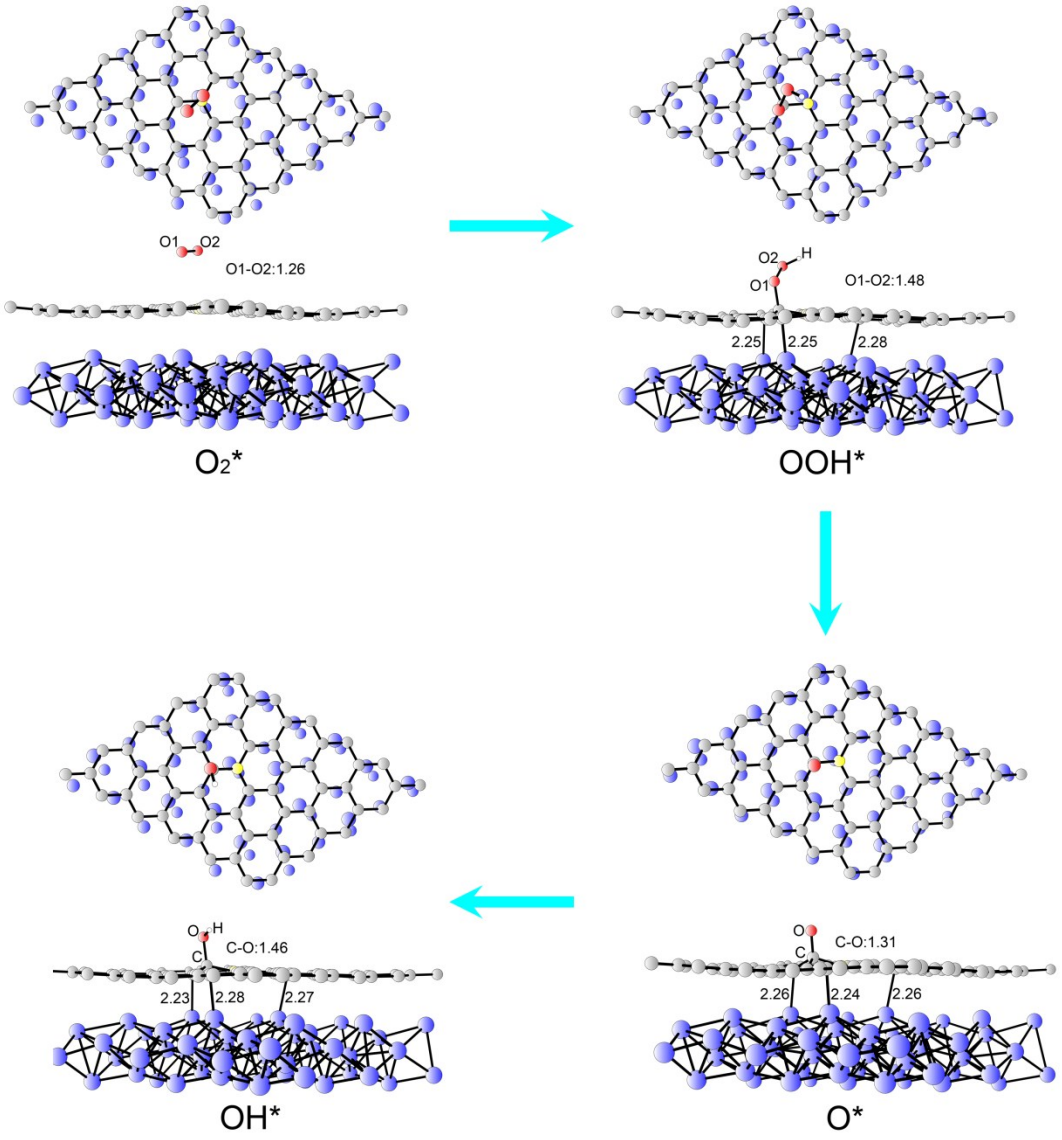

Fig. S14 Free-energy diagram for ORR on a negatively charged Co@GNG, Co@PNG and Pt (111) in alkaline(pH=13) media.

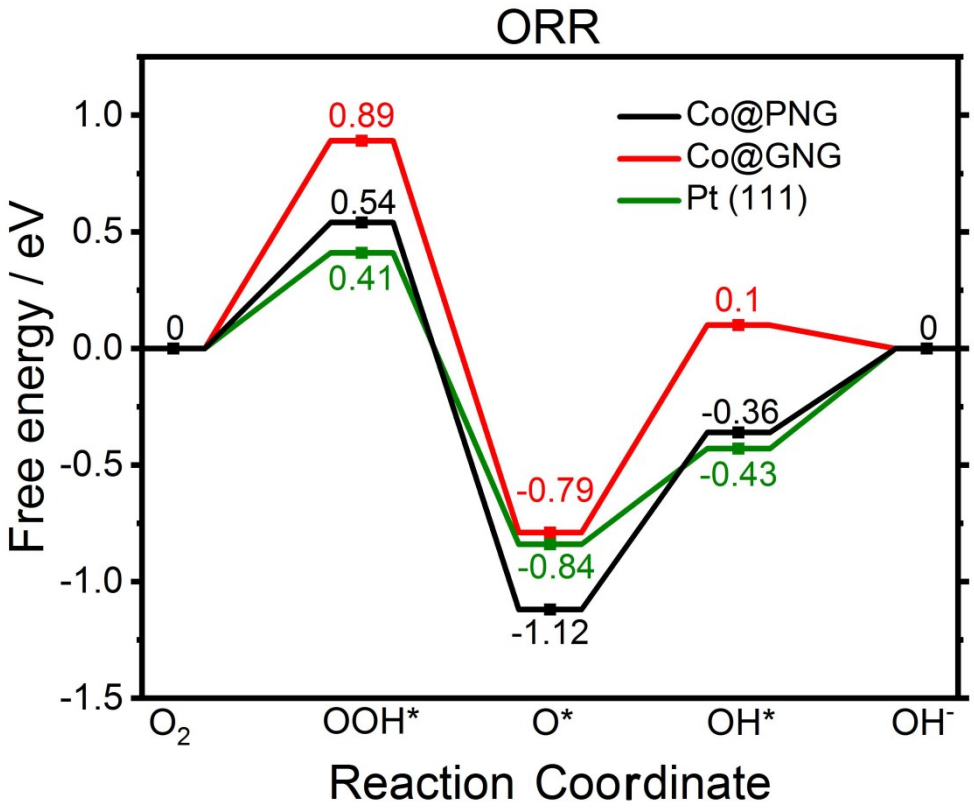

Fig. S15. Free-energy diagram for ORR on a negatively charged Co@GNG, Co@PNG and Pt (111) in alkaline(pH=13) media.

The free energy diagrams of ORR are shown in Fig. S15 (ESI†). It can be seen that a negatively charged Co@GNG is more active than Co@PNG for ORR with the energy barrier of 0.76 eV. Meanwhile, the performance of negatively charged Co@GNG is inferior to neutral Co@GNG.

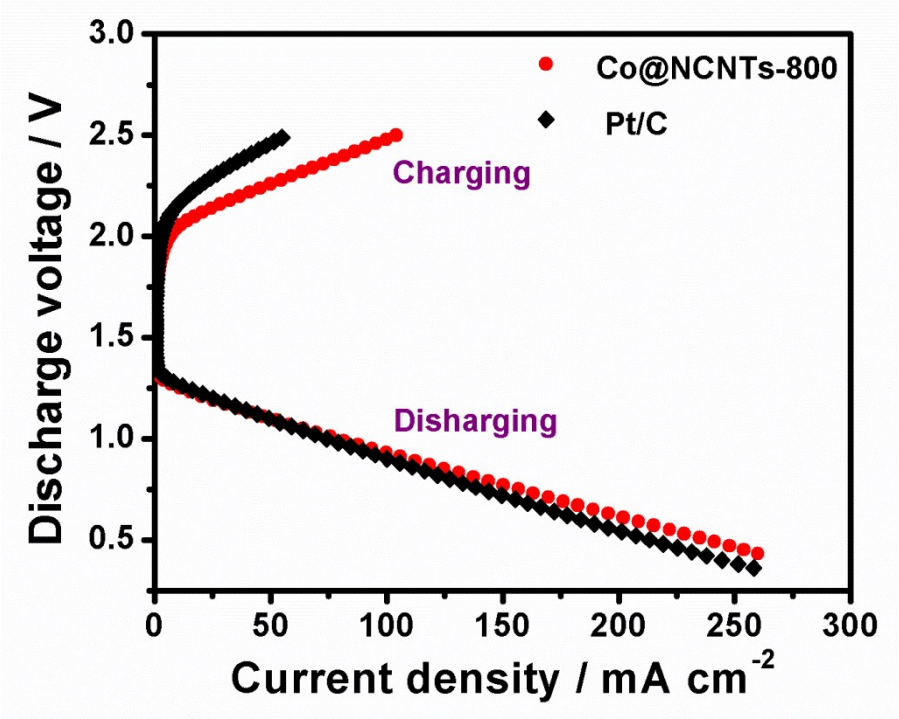

Fig. S16 Charging and discharging polarization curves.

Table S1 EXAFS fitting parameters at the Co K-edge for Co@NCNTs-800 and Co foil.

Sample	Shell	*CN* [a]	*R* (Å) [b]	σ^2 (Å^2·10^3) [c]	ΔE_0 (eV) [d]	*R* factor (%)
Co@NCNTs	Co-Co	7.4	2.49	5.3	6.7	0.88
Co foil	Co-Co	12	2.49	6.6	6.9	0.06

[a] *CN*: coordination numbers; [b] *R*: bond distance; [c] σ^2: Debye-Waller factors; [d] ΔE_0: the inner potential correction. *R* factor: goodness of fit. S_{02} for Co-Co is 0.78, were obtained from the experimental EXAFS fit of Co foil by fixing CN as the known crystallographic value.

Table S2. The comparison of ORR/OER activity of Co@NCNTs-800 and the other noble-metal-free electrocatalysts.

Catalysts	ORR E_{onset} (V)	ORR $E_{1/2}$ (V)	OER $E_{j=10\ mA\ cm^{-2}}$	Reference
Co@NCNTs-800	0.94	0.84	1.59	This work!
NGM-Co	0.88	0.79	1.74	*Adv. Mater.* **2017**, *29*, 1703185.
NC@Co-NGC DSNCs	0.92	0.82	1.64	*Adv. Mater.* **2017**, *29*, 1700874.
Co_3O_4/N-rGO	0.90	0.79	1.72	*Adv. Mater.* **2017**, *30*, 1703657
$Co_3FeS_{1.5}(OH)_6$	0.88	0.72	1.59	*Adv. Mater.* **2017**, *29*, 1702327
Co_4N/CNW/CC	0.92	0.73	1.54	*J. Am. Chem. Soc.* **2016**, *138*, 10226.
Ni_3Fe/N-C	0.95	0.76	1.60	*Adv. Energy Mater.* **2017**, *7*, 1601172.
NiO/CoN PINWs	0.89	0.68	1.53	*ACS Nano.* **2017**, *11*, 2275.
CoP-DC	0.90	0.81	1.57	*Adv. Energy Mater.* **2018**, *30*, 1703623
CoNi-SAs/NC	0.88	0.76	1.57	*Adv. Mater.* **2019**, DOI: 10.1002/adma.201905622

Reference

1. Liu, Q.; Wang, Y.; Dai, L.; Yao, J. *Adv. Mater.* **2016**, *28*, 3000-3006.
2. Perdew, J.; Urke, K.; Ernzerhof, M. *Phys. Rev. Lett.* **1996**, *77*, 3865-3868.
3. Kresse, G.; Joubert, D. *Phys. Rev. B* **1999**, *59*. 1758-1775.
4. Kresse, G.; Furthmüller, J. *Comp. Mater. Sci.* **1996**, *6*. 15-50.
5. Kresse, G.; Furthmüller, J. *Phys. Rev. B* **1996**, *54*, 11169-11186.
6. Abel, M.; Clair, S.; Ourdjini, O.; Mossoyan, M.; Porte, L. *J. Am. Chem. Soc.* **2011**, *133*, 1203-1205.
7. Grimme, S. *J. Comp. Chem.* **2006**, *27*, 1787-1799.
8. Yu, L.; Pan, X.; Cao, X.; Hu, P.; Bao, X. *J. Catal.* **2011**, *282*, 183-190.
9. Jiao, Y.; Zheng, Y.; Jaroniec, M.; Qiao, S. Z. *J. Am. Chem. Soc.* **2014**, *136*, 4394-4403.
10. Xu, H.; Cheng, D.; Cao, D.; Zeng, X. C. *Nat. Catal.* **2018**, *1*, 339-348.
11. Peterson, A. A.; Pedersen, F. A.; Studt, F.; Rossmeisl, J.; Nørskov, J. K. *Energy & Environ. Sci.* **2010**, *3*, 1311-1315.
12. Lim, D.-H.; Wilcox, J. *J. Phys. Chem. C* **2012**, *116*, 3653-3660.
13. Kattel, S.; Atanassov, P.; Kiefer, B. *J. Phys. Chem. C* **2012**, *116*, 8161-8166.
14. Wang, Y.; Yuan, H.; Li, Y.; Chen, Z. *Nanoscale* **2015**, *7*, 11633-11641.
15. Li, M.; Zhang, L.; Xu, Q.; Niu, J.; Xia, Z. *J. Catal.* **2014**, *314*, 66-72.
16. Nørskov, J. K.; Rossmeisl, J.; Logadottir, A.; Lindqvist, L.; Kitchin, J. R.; Bligaard, T.; Jo´nsson, H. *J. Phys. Chem. B* **2004**, *108*, 17886-17892.
17. Jia, Y.; Zhang, L.; Du, A.; Gao, G.; Chen, J.; Yan, X.; C. Brown, L.; Yao, X. *Adv. Mater.* **2016**, *28*, 9532-9538.
18. Yang, L.; Zeng, X.; Wang, D.; Cao, D. *Energy Storage Mater.* **2018**, *12*, 277-283.
19. Chen, X.; Wei, L.; Wang, Y.; Zhai, S.; Chen, Z.; Tan, S.; Zhou, Z.; Ng, A. K.; Liao, X.; Chen, Y. *Energy Storage Mater.* **2018**, *11*, 134-143.
20. Zhu, J.; Xiao, M.; Zhang, Y.; Jin, Z.; Peng, Z.; Liu, C.; Chen, S.; Ge, J.; Xing, W. *ACS Catal.* **2016**, *6*, 6335–6342.

21. Wei, L.; Karahan, H. E.; Zhai, S.; Liu, H.; Chen, X.; Zhou, Z.; Lei, Y.; Liu, Z.; Chen, Y. *Adv. Mater.* **2017**, *29*, 1701410-1701419.
22. Cheng, H.; Li, M. L.; Su, C. Y.; Li, N.; Liu, Z. Q.; *Adv. Funct. Mater.* **2017**, *27*, 1701833-1701842.
23. Su, C. Y.; Cheng, H.; Li, W.; Liu, Z. Q.; Li, N.; Hou, Z.; Bai, F. Q.; Zhang, H. X.; Ma, T. Y. *Adv. Energy Mater.* **2017**, *7*, 1602420-1602431.
24. Guo, Y.; Yuan, P.; Zhang, J.; Hu, Y.; Amiinu, I. S.; Wang, X.; Zhou, J.; Xia, H.; Song, Z.; Xu, Q.; Mu, S. *ACS Nano* **2018**, *12*, 1894-1901.
25. Wang, T.; Kou, Z.; Mu, S.; Liu, J.; He, D.; Amiinu, I. S.; Meng, W.; Zhou, K.; Luo, Z.; Chaemchuen, S.; Verpoort, F. *Adv. Funct. Mater.* **2017**, *28*, 1705048-1705056.
26. Zhang, M.; Dai, Q.; Zheng, H.; Chen, M.; Dai, L. *Adv. Mater.* **2018**, *30*, 1705431-1705440.
27. Fu, J.; Hassan, F. M.; Zhong, C.; Lu, J.; Liu, H.; Yu, A.; Chen, Z. *Adv. Mater.* **2017**, *29*, 1702526-1702534.
28. Liu, S.; Wang, Z.; Zhou, S.; Yu, F.; Yu, M.; Chiang, C. Y.; Zhou, W.; Zhao, J.; Qiu, J. *Adv. Mater.* **2017**, *29*, 1700874-1700883.
29. Wang, H. F.; Tang, C.; Wang, B.; Li, B. Q.; Zhang, Q. *Adv. Mater.* **2017**, *29*, 1702327-172335.
30. Jiang, Y.; Deng, Y. P.; Fu, J.; Lee, D. U.; Liang, R.; Cano, Z. P.; Liu, Y.; Bai, Z.; Hwang, S.; Yang, L.; Su, D.; Chu, W.; Chen, Z. *Adv. Energy Mater.* **2018**, *8*, 1702900-1702910.